ADVANCED MATERIALS
www.advmat.de

Electrical Dynamic Switching of Magnetic Plasmon Resonance Based on Selective Lithium Deposition

Yan Jin, Jie Liang, Shan Wu, Ye Zhang, Lin Zhou, Qianjin Wang, Hui Liu, and Jia Zhu**

Active plasmonic nanostructures have garnered considerable interest in physics, chemistry, and material science due to the dynamically switchable capability of plasmonic responses. Here, the first electrically dynamic control of magnetic plasmon resonance (MPR) through structure transformation by selective deposition of lithium on a metal–insulator–metal (MIM) structure is reported. Distinct optical switching between MPR and surface plasmon polariton (SPP) excitations can be enabled by applying a proper electrical current to the electrochemical cell. Furthermore, the structure transformation through lithium metal deposition indicates the reconfigurable MPR excitation in a full cycling of the charging and discharging process. The results may shed light on electrically compatible self-powered active plasmonics as well as nondestructive optical sensing for electrochemical evolution.

Dynamic plasmonics has generated tremendous excitements in the field of nanophotonics and metamaterials[1] due to active control of optical responses via either structure transformation[2] or material phase transition.[3] Because of the inherent self-built electric functionality, flexible modulation as well as compatibility, electrical control of metallic structures is of most importance among various dynamic control strategies[4] and widely employed to tune the electrical resonances in topologically continuous metallic structures, a new electrical reconfigurable route apart from the thermal and chemical effects.[4c,5,6] However, the magnetic metamaterial counterparts are rather challenging[3,7] to be electrically tuned because of discontinuous building blocks such as split ring resonators,[8] couple nanoparticles[9] and multiple stacked rods,[10] etc., which are desirable for operando monitoring for local structure dominating magnetic plasmon resonance (MPR) and pronounced magnetic field enhancement. Among various electrically switchable plasmonic devices, noble metals (including silver and gold) are most widely employed thus far, which are promising for distinct optical responses, stable chemical properties but should be maintained by continuous external power consumption.[11]

Alkali metals have long been predicted to be a promising plasmonic material with high density free electron gas, quite similar as silver.[12] The distinct low optical loss feature of alkali metals has recently been verified in sodium system through systematic demonstration of fundamental optical measurement as well as highly performing plasmonic devices at near-infrared wavelengths.[13] Besides, alkali metal including lithium and sodium has also been heavily investigated in the field of energy storage. Lithium metal anodes, as the lightest anode material for lithium-based batteries, possess the highest specific capacity of 3860 mAh g^{-1} and the lowest electrochemical potential (−3.04 V vs standard hydrogen electrode) to achieve high energy density.[14] It is expected that combining these two properties of lithium metal can represent exciting progress toward self-powered active plasmonic devices.

In this work, by taking advantage of two critical roles of lithium metal employed in the electric dynamic switching: the efficient optical information carrier and the holy grail energy storage carrier, we developed the first electrically dynamic switching of MPR based on a planar lithium metal battery. Our results provide a powerful strategy for reconfigurable magnetic metamaterials, shedding light on electrically compatible self-powered active plasmonics as well as nondestructive optical sensing for chemical reactions.

The proposed active switching of MPR is based on the electrically induced structure transformation of magnetic meta-atoms via the electrochemical evolution in a planar battery, as shown in **Figure 1**. In order to enable active control of MPR, there are three crucial components. First, the geometry-discontinuous magnetic meta-atoms are required to enable MPR excitations. Second, the electrically triggered structure transformation should be reproducible for controllable MPR switching. Third, in order to maximize optical contrast of MPR switching, an overall metallic structure with low optical loss is preferred. Here the silver-based metal–insulator–metal (MIM) structure is introduced on quartz substrate, the double metal strips of which can be utilized to induce the magnetic dipole moment. Silver is

Dr. Y. Jin, J. Liang, Y. Zhang, Prof. L. Zhou, Dr. Q. Wang, Prof. H. Liu, Prof. J. Zhu
National Laboratory of Solid State Microstructures
College of Engineering and Applied Sciences
School of Physics
Key Laboratory of Intelligent Optical Sensing and Manipulation
Ministry of Education
Jiangsu Key Laboratory of Artificial Functional Materials
Nanjing University
Nanjing 210093, P. R. China
E-mail: linzhou@nju.edu.cn; jiazhu@nju.edu.cn
Prof. S. Wu
Key Laboratory of Functional Materials and Devices for Informatics of Anhui Higher Education Institutes
Fuyang Normal University
Fuyang 236037, P. R. China
The ORCID identification number(s) for the author(s) of this article can be found under https://doi.org/10.1002/adma.202000058.

DOI: 10.1002/adma.202000058

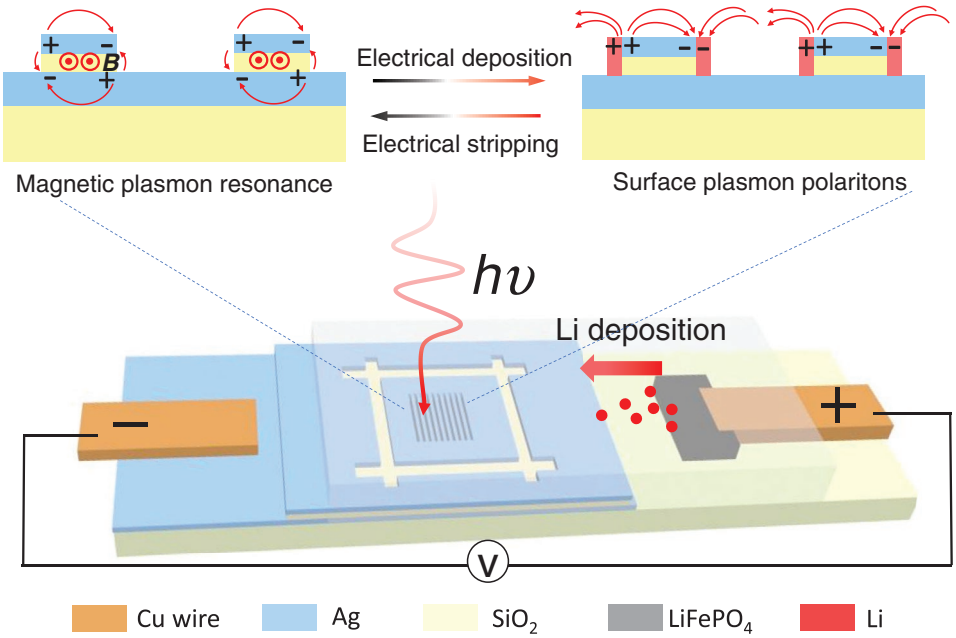

Figure 1. The schematic of electrically active switching of magnetic plasmon resonance via selective lithium deposition in the lithium metal battery.

finely chosen because of its low optical loss in the visible and near infrared as well as much higher selectivity of lithium nucleation than other metals.[14d,15] Once a proper electrical deposition current is applied, lithium ions extracted from $LiFePO_4$ source move toward the MIM patterned metasurface through liquid electrolyte. The high lithium deposition selectivity of silver can directionally guide the lithium metal depositing vertically along the sidewalls of the MIM,[16] leading to the structure transformation from MIM to continuous donut geometry. Based on the analysis of local charge oscillation, the transformation from the discontinuous to continuous meta-atom can enable the optical switching from localized magnetic excitations (MPR) to delocalized electric excitations (SPP) (upper panel in Figure 1).

We first calculated the optical responses of the two steady states of the electrically transformed plasmonic structures suggested in the top panel of Figure 1. All the calculations are based on the finite difference time domain (FDTD) method (see methods for details). As shown in **Figure 2**a that, the discontinuous MIM structure (the state before electrochemical lithium deposition, left top panel in Figure 1) is featured by the pronounced broad reflection dip at 1.85 µm, resembling the MPR spectroscopy feature, and a slight dip at around 800 nm of hybrid SPP excitation, which is adjacent to the little kink due to Rayleigh anomaly.[17] Once the metallic donut (the state after electrochemical lithium deposition, right top panel in Figure 1) forms, the dip at 1.85 µm completely disappears, while a sharp dip at ≈1 µm emerges, which is redshifted from 800 nm, in close proximity to the SPP excitation on the metal/dielectric interface.[18] The difference of SPP between disconnected (before lithium deposition) and connected (after lithium deposition) structures is the Fourier coefficient (or called as the modulation strength) of the periodic structure.[17] One may further identify the nature of MPR (≈1.85 µm) and SPP (≈1 µm) from the electromagnetic field distribution profiles, shown in Figure 2b and Figure S1 (Supporting Information). For the MPR mode, the excited reflectance dip at 1.85 µm before lithium deposition possesses antiparallel electric dipole pairs across the double silver layers (see the E_z profiles, upper panel in Figure 2b), leading to an artificial magnetism (see J profile, upper panel in Figure 2b) and a pronounced magnetic field enhancement in the spacing SiO_2 film (so called MPR). However, after lithium deposition, the MPR mode at the same frequency (1.85 µm) disappears (Figure S1a,b, Supporting Information), which demonstrates the dynamic control of MPR through structure transformation. Besides, the calculated field profiles for the SPP modes before and after lithium deposition are shown in lower panels in Figure 2b and Figure S1 (Supporting Information). Before lithium deposition, surface mode SPP excitation on the air/MIM surface can exist because of the periodicity of MIM structure (Figure S1c,d, Supporting Information). Furthermore, as the bottom and upper silver strips are connected after lithium deposition, the connected MIM structure behaves like a semi-infinite metal/dielectric grating, on which the hybrid propagating SPP mode is excited (lower panels in Figure 2b).[18] Hence, the electrically triggered discontinuous-to-continuous structure transformation plays the crucial role in the active plasmonic switching between localized MPR and delocalized SPP.

In order to identify the functionality of electrically switchable MPR proposed in Figure 2, we first performed the ex situ reflectance measurements. We measured the reflectance spectrum of the MIM structure before and after 5 min electrochemical deposition of lithium metal at an applied current of 300 µA, respectively, as shown in **Figure 3**. One may find that, the measured reflectance spectrum (Figure 3b) of the pre-patterned MIM structure (Figure 3a) before lithium deposition exhibits a distinct reflection dip at around 1.85 µm, far from the delocalized SPP excitation related to the periodic structure (≈790 nm), which is a bit beyond the acquirable spectral region of the microscopic reflectance detector. In addition, the distinct reflection dip possesses a broad bandwidth as well as symmetric

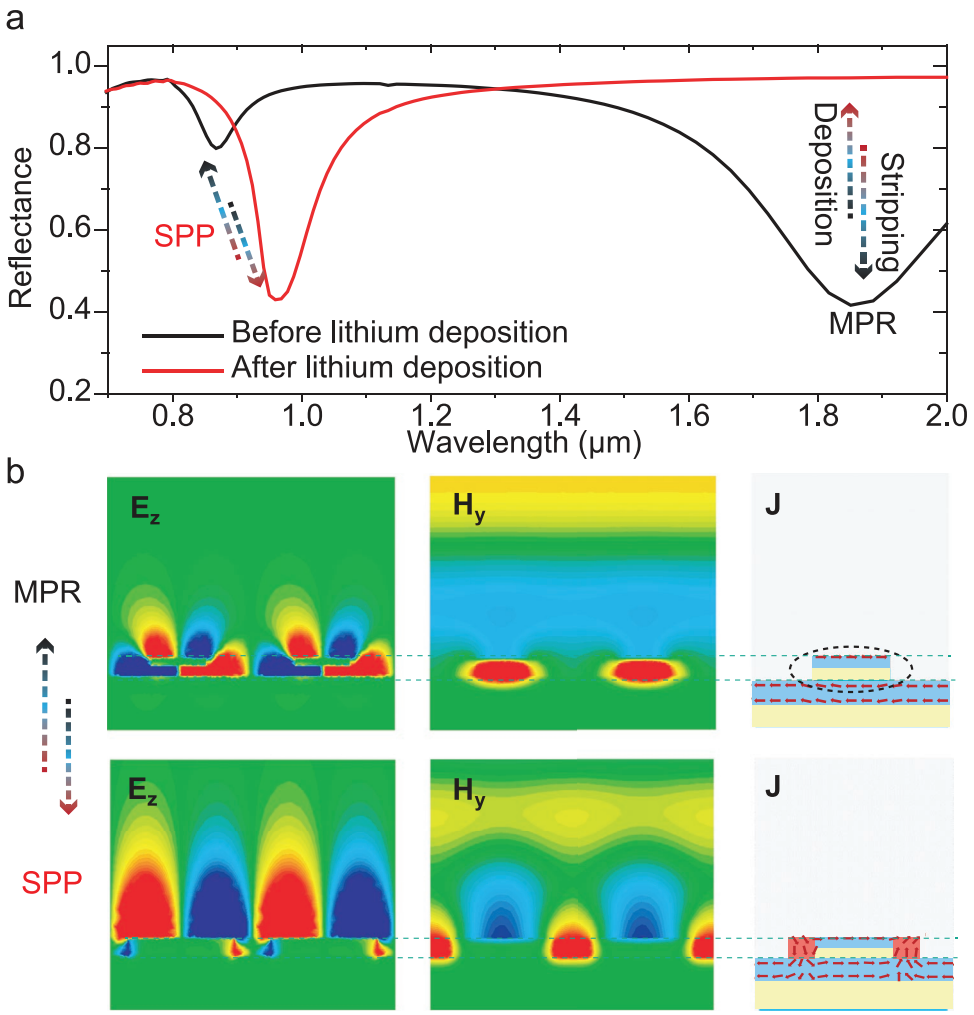

Figure 2. Calculated reflection spectra and field distributions. a) Calculated reflection spectra of the two representative metallic structures before and after lithium deposition, respectively. The period and strip width of MIM are $P = 790$ nm and $L_m = 400$ nm, respectively. The thickness of top and bottom silver layer are $d_{m1} = 50$ nm and $d_{m2} = 100$ nm with $d_i = 50$ nm SiO_2 as the spacing layer. The lithium width is 100 nm on each side after deposition. b) Calculated electric field E_z, magnetic field H_y and current density J field distributions of the MPR (upper panel) and SPP (lower panel) mode, respectively.

profile, indicating the MPR feature. Note that the little difference between the measured resonance wavelength compared with the calculated one (Figure 2a) could be ascribed to the FIB fabrication process for the nonvertical edge of the groove,[19] leading to slightly changed geometry parameters (period: $P = 790$ nm, strip width: $L_m = 400$ nm). After a period of lithium deposition, the silver-based MIM sandwich will induce lithium metal growth vertically along the MIM sidewalls, leading to the conformal expansion of MIM with connected silver strip pairs. As observed from the SEM image in Figure 3c, the average stripe width increases from 400 to 500 nm after lithium deposition at 300 μA for 5 min. (Note: lithium deposition along the sidewall is demonstrated in the cross-sectional SEM images after lithium deposition, see Figure S2, Supporting Information) As a result, after the deposition induced MIM structure transformation, the MPR mode around 1.85 μm disappears while an enhanced hybrid SPP mode with an asymmetric sharp dip redshifts to around 1 μm (Figure 3d). These electrically switchable ex situ results show good agreement with the numerical calculations in Figure S3 (Supporting Information) as well as the conceptual design in Figure 2a, proving the validity of the electrically switchable MPR based on lithium deposition.

To further demonstrate the reconfigurable switchability of MPR, we conducted in situ reflectance measurement of the MIM structure in a full electrochemical cycle, aiming at revealing the correlation between the nanoscale lithium morphology and spectroscopy during the dynamic process of lithium deposition. The battery voltage during cycling is recorded in **Figure 4**a. As shown in Figure 4b, before lithium deposition, there are two dips (≈1.2 and ≈1.6 μm) which are due to SPP (on metal/electrolyte interface) and MPR respectively, resembling the primary features of the ex situ experiments. The dip locations are different from the ex situ experiments due to the FIB process and electrolyte environment, demonstrated in Figure S4a (Supporting Information). When lithium begins to deposit after a 300 μA electrical current is applied, the two representative dynamic evolution rules in the ex situ case (the on/off switching of MPR and the slight redshift of SPP, Figure 3) are mostly reproduced in the in situ experiment (Figure 4) and corresponding simulations in Figure S4 (Supporting Information).

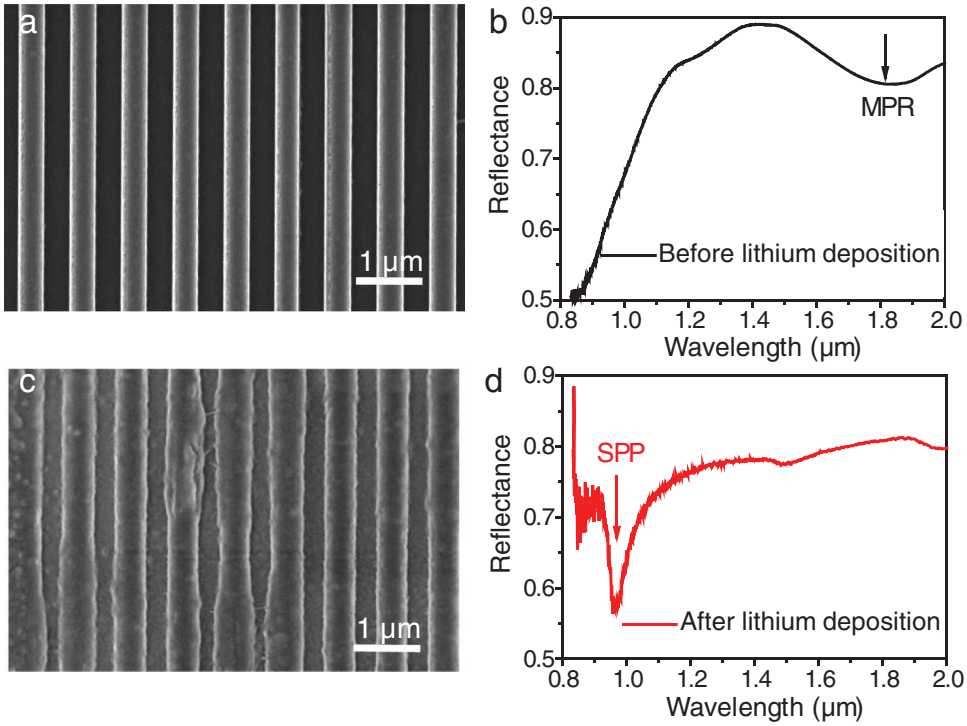

Figure 3. Ex situ reflection characterization during normal lithium deposition in Ag–SiO_2–Ag MIM structure. a) SEM image of the original MIM structure with period ≈790 nm and metal strip width ≈400 nm. b) Reflectance curve before lithium deposition. c) SEM image of MIM structure after lithium deposition at 300 μA for 5 min. d) Reflectance curve after lithium deposition at 300 μA for 5 min.

First, the on/off/on switching of MPR at ≈1.6 μm is observable during a full cycle in the experiment. The redshift of MPR toward 1.85 μm (after lithium deposition) is due to the discontinuous point-like vertical deposition along MIM ridges (demonstrated in Figure S4b, Supporting Information). Secondly, the SPP dip is slightly redshift and finally recovered after the full cycle, which is well reproduced in both the in situ experiments (see shallow dips ≈1.3 μm Figure 4b,c) and the simulated in situ evolution curves (see dips ≈1.3 μm Figure S4b,c, Supporting Information). The SPP dip at 1.3 μm is less observable in the depositing evolved spectra probably due to reduced long range periodicity of the structure. Similar case happens nearby $\lambda \approx 1\,\mu m$ (a newly emerged reflection dip shown in Figure S5, Supporting Information), which will be discussed later. Once the applied current is reversed, lithium metal is stripped from the MIM structure (Figure 4c). During this process, a smaller current of 100 μA is applied so as to fully extract the lithium metal with relatively higher columbic efficiency. During lithium stripping process, the intensity of reflectance dip due to MPR excitation become stronger and the dip gradually blueshifted back. As it approaches the end of stripping, the reflectance dip around 1.6 μm appears again, indicating the lithium stripping process almost completely transforms the semi-infinite metallic grating back into the MIM structure. Note that the remaining reflection dip at ≈1 μm (Figure S5, Supporting Information) after a full cycle suggests that this newly generated dip is probably originated from heterogeneous deposition and/or side reactions (Note S1, Supporting Information). Such incomplete lithium stripping is widely known as dead lithium in the first cycle due to the low initial coulombic efficiency. The demonstrated in situ reflectance spectra suggested that the electrical switched MPR is reconfigurable, which can be employed as nondestructive optical sensor for electrochemical reactions. Compared with the previously reported SPP-based optical sensing system,[5a] MPR commonly possesses much longer resonant wavelength (far from the intrinsic interband absorption), beneficial for higher optical contrast. In addition, the quite different angular dependent spectroscopy feature of the MPR (before deposition) compared with SPP (after deposition) can provide distinct optical signature for detecting the electrochemical lithium metal evolution process.[20]

Finally, we would like to discuss the selectivity of metal substrate for the transformation of MIM structure. A widely used anode current collector material (copper) is employed as a comparison of silver. The ex situ reflectance of Cu-based MIM is shown in Figure S6 (Supporting Information). One may find that the lithium deposition in Cu-MIM is almost out of control (random dendrite growth, Figure S6d, Supporting Information) when applying the same current (300 μA) as in Ag-MIM structure, which can be ascribed to much lower solubility of lithium in copper and thus larger overpotential for uncontrolled lithium nucleation and dendrite morphology formation. Therefore, the reconfigurable electrical switch of MPR can be enabled by well controlling the electric current as well as deposition overpotential.

In summary, we demonstrate the first self-powered electrical dynamic switching of MPR based on lithium metal deposition in a lithium metal battery. With precisely designed silver-based MIM structure, the dynamic optical switching between MPR and SPP excitations are realized via electrochemical charging

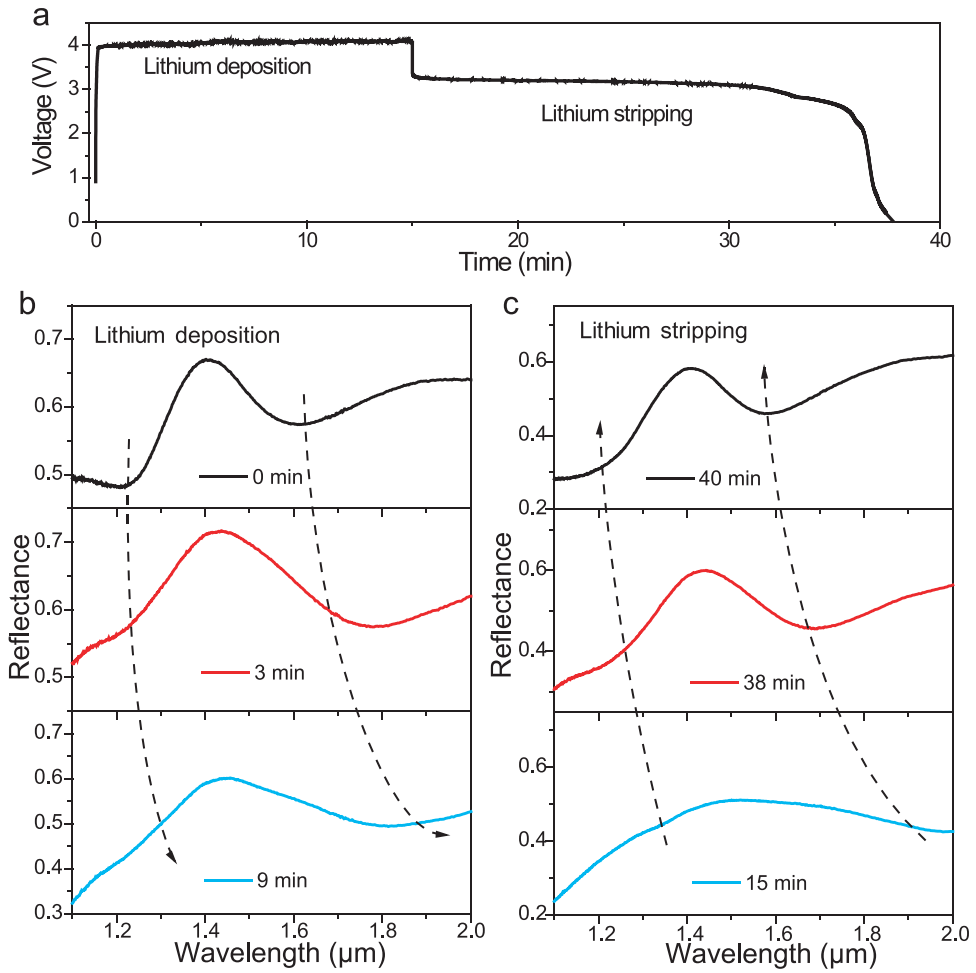

Figure 4. In situ reflection characterization of Ag–SiO_2–Ag MIM structure during electrochemical cycling. a) Battery voltage during lithium deposition and stripping process. b) In situ reflectance curve during lithium deposition at 300 μA. c) In situ reflectance curve during lithium stripping at 100 μA.

and discharging process, leading to reconfigurable structure transformation from discontinuous MIM to semi-infinite metallic grating. The morphology correlated reflectance spectroscopy can serve as a research platform for electrically active plasmonics, paving an alternative way to nondestructive optical sensing for in situ chemical reactions.

Experimental Section

Planar Battery Fabrication: The MIM structure was obtained in two steps: layer metal (Ag or Cu), dielectric (SiO_2 or MgF_2) and metal (Ag or Cu) film with a thickness of 100, 50, and 50 nm was deposited on a SiO_2 wafer (thickness ≈ 1 mm) through physical vapor deposition (PVD, Gatan 682). The MIM structure was fabricated by FIB (Dual-beam FIB 235, FEI Strata). During in situ test, planar battery was made up with 3 components: MIM structure on one side, $LiFePO_4$ electrode on the other side and liquid electrolyte (1.0 M $LiPF_6$ in 1:1 vol/vol ethylene carbonate/diethyl carbonate with 2 wt% vinylene carbonate, Guotaihuarong Corporation). The battery was covered by another transparent glass and sealed with epoxy resin.

Characterization: A system based on a micro-spectrophotometer (Bruker vertex 70) is employed to acquire the reflection spectra. An electrochemical workstation (Biologic SP-20) is used to control the lithium deposition/stripping through galvanostatic cycling and measure the time-dependent potentials. For the ex situ reflection test, lithium deposition is finished in glove box and MIM structure sample is sealed by another glass with epoxy resin for reflection test (without electrolyte). The area without grating is used as the reference. During the in situ reflection test, the planar battery with electrolyte is employed and the area without grating soaking in electrolyte is used as the reference. The morphologies and structures during the fabrication processes and lithium deposition were characterized by scanning electron microscopy (Dual-beam FIB 235, FEI Strata). During ex situ characterization of the lithium morphology, the battery was opened in the Ar glove box after lithium deposition and optical reflectance measurement, and the electrode was then rinsed with fresh diethyl carbonate and dried. Electrodes were mounted onto SEM stages and sealed in an Ar-filled transfer container for immediate SEM observation.

Numerical Simulation: The finite-difference time-domain method was used to calculate the reflectance spectra as well as the electric field E_z, magnetic field H_y and current density vector J of two representative microstructures, respectively. For simplicity, periodic boundary condition is used for the modeling and plane wave is employed as the excitation source. The material parameters of lithium metal and silver are from the Palik data, and the refractive index of SiO_2 and electrolyte are set as 1.45 and 1.4 respectively. The thickness of lithium is used to correlate to the lithium metal evolution process in the experiment. For the ex situ simulation, the period is set as 790 nm. The widths of upper silver layer and SiO_2 layer are 400 nm, and the width of lithium metal is set as 100 nm on each side.

Supporting Information

Supporting Information is available from the Wiley Online Library or from the author.

Acknowledgements

Y.J. and J.L. contributed equally to this work. The authors acknowledge the micro-fabrication center of National Laboratory of Solid State Microstructures (NLSSM) for technique support. This work is jointly supported by the National Key Research and Development Program of China (No. 2017YFA0205700), National Natural Science Foundation of China (Nos. 11874211, 61735008, 51925204), and the Fundamental Research Funds for the Central Universities (Nos. 021314380150, 021314380140).

Conflict of Interest

The authors declare no conflict of interest.

Keywords

electrical switching, lithium metal deposition, magnetic plasmon resonance, metal–insulator–metal (MIM) structure, surface plasmons

Received: January 3, 2020
Revised: June 28, 2020
Published online:

[1] a) N. Jiang, X. Zhuo, J. Wang, *Chem. Rev.* **2018**, *118*, 3054; b) A. Nemati, Q. Wang, M. Hong, J. Teng, *Opto-Electron. Adv.* **2018**, *1*, 18000901.
[2] A. V. Krasavin, N. I. Zheludev, *Appl. Phys. Lett.* **2004**, *84*, 1416.
[3] W. X. Huang, Y. Zhang, X. M. Tang, L. S. Cai, J. W. Zhao, L. Zhou, Q. J. Wang, C. P. Huang, Y. Y. Zhu, *Opt. Lett.* **2011**, *36*, 3359.
[4] a) X. Duan, S. Kamin, F. Sterl, H. Giessen, N. Liu, *Nano Lett.* **2016**, *16*, 1462; b) P. Yu, J. Li, S. Zhang, Z. Jsin, G. Schütz, C. W. Qiu, M. Hirscher, N. Liu, *Nano Lett.* **2018**, *18*, 4584; c) X. Duan, S. Kamin, N. Liu, *Nat. Commun.* **2017**, *8*, 14606; d) Y. Wu, W. Yang, Y. Fan, Q. Song, S. Xiao, *Sci. Adv.* **2019**, *5*, eaax0939.
[5] a) Y. Jin, L. Zhou, J. Yu, J. Liang, W. Cai, H. Zhang, S. Zhu, J. Zhu, *Proc. Natl. Acad. Sci. USA* **2018**, *115*, 11168; b) C. Novo, A. M. Funston, A. K. Gooding, P. Mulvaney, *J. Am. Chem. Soc.* **2009**, *131*, 14664.
[6] a) Y. X. Wang, H. Liu, Z. Q. Li, X. X. Zhang, R. K. Zheng, S. P. Ringer, *Appl. Phys. Lett.* **2006**, *89*, 042511; b) J. Z. Hu, H. K. Yu, G. X. Su, B. X. Song, J. Wang, Z. Q. Wu, P. Zhan, F. X. Liu, W. Wu, Z. L. Wang, *Adv. Opt. Mater.* **2020**, *8*, 1901305; c) S. Zhang, W. Fan, K. Malloy, S. Brueck, N. Panoiu, R. Osgood, *Opt. Express* **2005**, *13*, 4922.
[7] L. Kang, S. Lan, Y. Cui, S. P. Rodrigues, Y. Liu, D. H. Werner, W. Cai, *Adv. Mater.* **2015**, *27*, 4377.
[8] a) M. Decker, R. Zhao, C. M. Soukoulis, S. Linden, M. Wegener, *Opt. Lett.* **2010**, *35*, 1593; b) N. Liu, H. Liu, S. Zhu, H. Giessen, *Nat. Photonics* **2009**, *3*, 157.
[9] M. Hentschel, L. Wu, M. Schäferling, P. Bai, E. P. Li, H. Giessen, *ACS Nano* **2012**, *6*, 10355.
[10] Y. Zhao, M. A. Belkin, A. Alu, *Nat. Commun.* **2012**, *3*, 870.
[11] a) Z. Feng, C. Jiang, Y. He, S. Chu, G. Chu, R. Peng, D. Li, *Adv. Opt. Mater.* **2014**, *2*, 1174; b) A. Tsuboi, K. Nakamura, N. Kobayashi, *Adv. Mater.* **2013**, *25*, 3197; c) G. Wang, X. Chen, S. Liu, C. Wong, S. Chu, *ACS Nano* **2016**, *10*, 1788.
[12] a) M. Blaber, M. Arnold, N. Harris, M. Ford, M. Cortie, *Phys. B* **2007**, *394*, 184; b) M. G. Blaber, M. D. Arnold, M. J. Ford, *J. Phys.: Condens. Matter* **2010**, *22*, 143201.
[13] Y. Wang, J. Yu, Y. F. Mao, J. Chen, S. Wang, H. Z. Chen, Y. Zhang, S. Y. Wang, X. Chen, T. Li, L. Zhou, R. M. Ma, S. Zhu, W. Cai, J. Zhu, *Nature* **2020**, *581*, 401.
[14] a) J. Liu, Z. N. Bao, Y. Cui, E. J. Dufek, J. B. Goodenough, P. Khalifah, Q. Y. Li, B. Y. Liaw, P. Liu, A. Manthiram, Y. S. Meng, V. R. Subramanian, M. F. Toney, V. V. Viswanathan, M. S. Whittingham, J. Xiao, W. Xu, J. H. Yang, X. Q. Yang, J. G. Zhang, *Nat. Energy* **2019**, *4*, 180; b) X. Wu, J. Wang, D. Fei, X. Chen, E. Nasybulin, Y. Zhang, J. G. Zhang, *Energy Environ. Sci.* **2014**, *7*, 513; c) C. P. Yang, Y. X. Yin, S. F. Zhang, N. W. Li, Y. G. Guo, *Nat. Commun.* **2015**, *6*, 8058; d) K. Yan, Z. D. Lu, H. W. Lee, F. Xiong, P. C. Hsu, Y. Z. Li, J. Zhao, S. Chu, Y. Cui, *Nat. Energy* **2016**, *1*, 16010.
[15] P. R. West, S. Ishii, G. V. Naik, N. K. Emani, V. M. Shalaev, A. Boltasseva, *Laser Photonics Rev.* **2010**, *4*, 795.
[16] M. H. Ryou, Y. M. Lee, Y. J. Lee, M. Winter, P. Bieker, *Adv. Funct. Mater.* **2015**, *25*, 834.
[17] a) W. Cai, U. K. Chettiar, H. K. Yuan, V. C. de Silva, A. V. Kildishev, V. P. Drachev, V. M. Shalaev, *Opt. Express* **2007**, *15*, 3333; b) M. H. Lu, X. K. Liu, L. Feng, J. Li, C. P. Huang, Y. F. Chen, Y. Y. Zhu, S. N. Zhu, N. B. Ming, *Phys. Rev. Lett.* **2007**, *99*, 174301.
[18] L. Zhou, C. P. Huang, S. Wu, X. G. Yin, Y. M. Wang, Q. J. Wang, Y. Y. Zhu, *Appl. Phys. Lett.* **2010**, *97*, 011905.
[19] L. Zhou, Q. J. Wang, S. Wu, W. X. Huang, C. P. Huang, Y. Y. Zhu, *J. Opt. Soc. Am. B* **2011**, *28*, 587.
[20] C. J. Tang, P. Zhan, Z. S. Cao, J. Pan, Z. Chen, Z. L. Wang, *Phys. Rev. B* **2011**, *83*, 041402.